CFD ANALYSIS AND PARAMETRIC STUDY-OPTIMIZATION OF SUCTION-BLOWING FLOW CONTROL TECHNIQUES

X. Trompoukis, V. G. Asouti, T. Zervogiannis and K. C. Giannakoglou[1]

[1]Lab of Thermal Turbomachines,
Department of Mechanical Engineering,
National Technical University of Athens,
P.P Box 64069, 15710, Athens, Greece
e-mail: kgianna@central.ntua.gr ; web page: velos0.ltt.mech.ntua.gr/research

Keywords: Computational Fluid Dynamics, Active Flow Control, Flow Separation, Synthetic Jets.

Abstract. *This paper is concerned with numerical predictions of active flow control techniques (pulsating jet, and steady suction) that are capable of suppressing flow separation regions in decelerating boundary layers. A parallel Navier-Stokes solver with one- or two-equation turbulence models and the appropriate boundary conditions, accompanied by the necessary unstructured grid generator, is used for the analysis or optimization (acting as the evaluation tool guided by a search method) of active flow control techniques. This software is first validated on benchmark cases, by comparing our numerical predictions with measurements. The parametric study of a flow control configuration, using the validated tool, follows. A step-by-step "optimization" is carried out, in which the slot location and geometry as well as the blowing/suction characteristics are sequentially selected to maximize the reduction in viscous flow losses.*

1 FLOW CONTROL - INTRODUCTION

During the last years, flow control techniques have gained particular attention. In airfoil aerodynamics, flow control may postpone or even prevent separation, leading to enhanced lift (without flap deflections or other high lift devices) and improved performance. Depending on energy requirements, passive (no extra power needed) and active (with extra power expenditure) control techniques have been developed. The most frequently used passive control technique is through vortex generators (with various shapes and scales) that produce longitudinal vortices contributing to the exchange of momentum between the near wall region and the outer flow. On the other hand, active flow control mechanisms, mostly in the form of suction or blowing slots optimally arranged over the solid wall, add steady or unsteady energy to the flow. Beyond steady suction or blowing, the use of synthetic jets, i.e. the interleaving use of blowing and suction with zero efflux has recently been proposed. This paper focuses on pulsating jets and steady suction. Note that it is beyond the scope of this paper to discuss interactive micro-electromechanical control techniques (MEMS), where control is carried out by integrated micro-actuators depending on the continuously updated input from micro-sensors; the interested reader should refer to [1].

The use of flow separation control techniques, based on suction and/or blowing, requires the understanding of near wall flow features, a software to accurately model the relevant flow physics and an optimization process to determine the best performing configuration. Several numerical investigations using steady or unsteady Navier-Stokes solvers for compressible or incompressible fluids and various turbulence models, with or without optimization actions, can be found in the literature; see [2] and [3], to report just a few of them. In [2], the configuration proposed in [4] was studied by testing several jet parameters. In [3], the optimization of the control parameters of a synthetic jet (slot location, frequency actuation, momentum coefficient) over the NACA 0015 airfoil which led to a considerable increase in lift and delay of stall, is presented.

The work presented in this paper is divided in two parts. In the first part, an in-house parallel (U)RANS solver is adapted to take into account the presence of flow control. This code may handle 2D flow domains discretized using unstructured meshes, on which the steady or unsteady Navier-Stokes equations are solved using various turbulence models. The use of unstructured grids is very convenient for the problem under consideration, where the flow area (and grid) must also include a cavity underneath the suction or blowing slot. In addition, the use of automatically generated unstructured meshes facilitates a lot the remeshing process during the search for optimal solutions. Before proceeding to the parametric study and optimization, the adapted software was validated on a benchmark case (from the CFDVal2004 Workshop, [5]) with a synthetic jet case over a wall-mounted hump and steady or unsteady flow control. Pressure coefficient distributions are compared to available measurements.

In the second part, a new wall geometry with similarities to that of the CFDVal2004 Workshop, was

generated; this shape was chosen so as to cause massive separation. Using steady suction on a fixed wall shape, the reduction of the separation length depends on four parameters, namely the location of the suction slot, its width, the jet inclination with respect to the local wall normal and the suction velocity. Since the optimization using a stochastic search algorithm is extremely costly due to the computationally demanding evaluations, a "ceteris paribus optimization" approach driven by a step-by-step parametric study was used instead. This is a sequential "optimization" procedure where the design variables are investigated one-by-one: the optimal value of the first design parameter is found and kept frozen during the search for the optimal value of the second parameter and so forth.

2 THE CFD TOOL

2.1 The Unsteady Reynolds-Averaged Navier-Stokes (URANS) Solver

The URANS code solves the Navier-Stokes equations, in conservative form, as

$$\frac{\partial \vec{U}}{\partial t} + \frac{\partial \vec{F}_i^{inv}}{\partial x_i} - \frac{\partial \vec{F}_i^{vis}}{\partial x_i} = 0 \tag{1}$$

where $\vec{U}$ is the vector of conservative variables and $\vec{F}_i^{inv}$, $\vec{F}_i^{vis}$ are the inviscid and viscous fluxes respectively. A finite volume, second-order in both time and space, vertex-centered upwind scheme on unstructured grids with triangular elements is used, [6]. A typical finite volume is defined in fig. 1. The inviscid flux crossing the interface between the volumes centered at two adjacent nodes (such as P and Q, associated with a normal vector $\vec{n}$) is computed by solving a 1D Riemann problem, using the Roe scheme, [7]; second-order accuracy is obtained through variables' extrapolation. The least squares method coupled with the Venkatakrishnan [8] limiter was used for the reconstruction of the variables at the finite volumes' interfaces. The viscous fluxes are computed by assuming linear distribution of the primitive flow variables within each triangle, an assumption that leads to a constant viscous flux vector within each element. To deal with turbulent flows, various one- and two-equation turbulence models can be used; in [9] the reader may find a list of the available turbulence models. Dual (real and pseudo) time-stepping is employed. The numerical solution of the discretized flow equations between two successive (real) time steps is carried out by repetitively using the point implicit Jacobi method. In the following studies, the steady state counterpart of this software was used for numerically predicting steady suction cases. The flow solver is fully parallel, based on the multi-domain technique, and the PVM or MPI protocols.

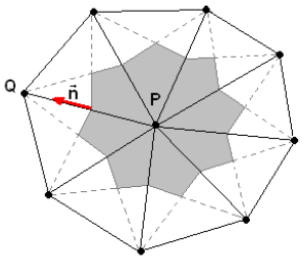

Figure 1: Finite volume surrounding grid node P of an unstructured grid with triangular elements.

2.2 Implementation of Boundary Conditions at the Suction/Blowing Slot

For either pulsating jets or steady suction, which are the two cases concerned herein, the boundary conditions determining the flow actuation are imposed after attaching a bell-shaped cavity to the slot. At the lower boundary of the cavity (inflow/outflow boundary, fig. 2), these boundary conditions are imposed using the flux-vector scheme (FVS), which is also used for the imposition of the inflow/outflow conditions at the main flow domain.

In the steady suction case, the numerical fluxes crossing any part of the cavity outlet are computed by employing FVS between the boundary node and a fake node where the $\rho V_n = \frac{\dot{m}_{jet}}{A_{cavout}}$ value (ρ is the density, V_n is the normal to the boundary velocity component, $\dot{m}_{jet}$ is the suction mass flow rate and A_{cavout} is the area of the cavity outlet) is imposed; the remaining flow quantities at the fake node are all extrapolated from the interior nodes.

In the case of pulsating jets, a sinusoidal actuation is assumed; so, practically, the inflow-outflow velocity is

given by $\rho V_n = \frac{\dot{m}_{jet}}{A_{cavout}} \sin(2\pi f t)$, where f is the actuation frequency. Depending on the sign of ρV_n, suction or blowing conditions are instantaneously imposed. During the suction phase of the actuation period, the boundary conditions are imposed as in steady suction case, using the instantaneous normal mass flow rate value. During the blowing phase, the ρ value must also be imposed at the fake nodes.

2.3 Validation of the Adapted Software on the CFDVal2004 Hump Case

The benchmark hump geometry and cavity are shown in fig. 2 (top). The inlet Mach number is 0.1 and the Reynolds number based on the hump chord is $9.36 \cdot 10^5$. The case was examined three times, (a) without flow control, (b) with steady suction, $\dot{m}_{jet} = 0.01518 kg/s$ per unit depth and (c) with a pulsating jet, $f = 138.5 Hz$, $V_{jet} = 26.6 m/s$, $c_\mu = 0.111\%$. Here, c_μ is the oscillatory flow momentum coefficient. Note that the jet velocity V_{jet} is defined at the slot and is obviously different than the aforementioned normal velocity V_n at the cavity inlet/outlet, where the area is much larger than at the slot. In the steady suction case, the k-ε (its low Reynolds variant by Chien), k-ω (the baseline, BSL, and shear-stress transport, SST, variants) and the Spalart-Allmaras (SA) turbulence models were tested; practicalities about the model implementation and the relevant references can be found in [9]. Numerical results for all cases, in the form of pressure coefficient (c_p) plots, can be found in fig. 3. In the uncontrolled case, the present CFD results are in accordance with CFD results by other researchers presented in the Workshop (not repeated here). As mentioned in [10], CFD methods miss the pressure levels over the hump and predict higher pressures than the experimental. This is due to the blockage effects caused by the side plates in the experiment, and as shown in fig. 3 (left), our results are closer to the measurements without side plates. For the steady suction case (fig. 3, mid), the present results overpredict the pressure level along the fore-body. Also, the pressure distributions in the separated region (over the ramp) have slightly different shapes and levels compared to the experimental results. The same tendency can be recognized in other CFD results present at the workshop and this discrepancy is also attributed to the blockage effects of side walls, [10]. The discrepancies among predictions based on different turbulence models are expected. Finally, for the oscillatory case (fig. 3, right), the results presented herein have the same trends as those presented at the workshop [5].

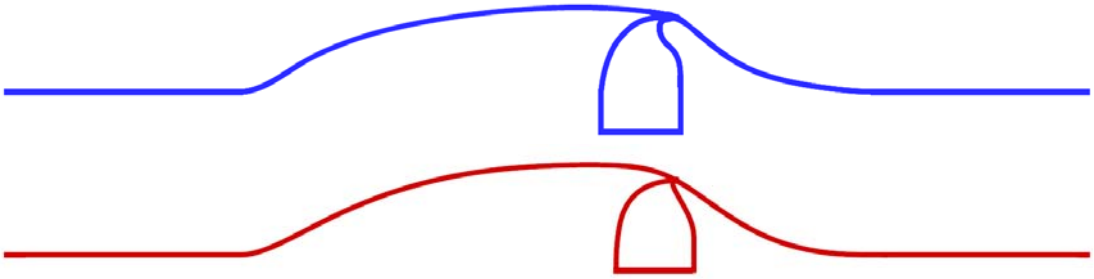

Figure 2: (a) Hump and cavity geometry; CFDVal2004 Workshop benchmark.
(b) Hump and cavity geometry; the new benchmark.

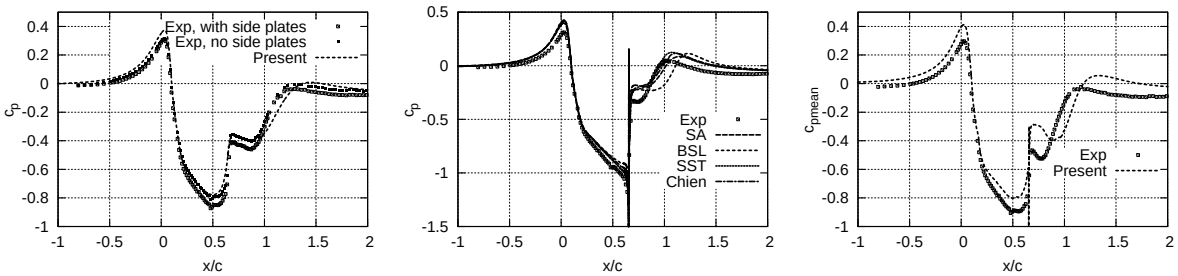

Figure 3: Validation of the flow solver with no flow control (left), steady suction (mid) and pulsating suction/blowing (right): pressure coefficient plots of CFD results together with the corresponding experimental data.

3 A STEADY SUCTION CASE – PARAMETRIC STUDY

3.1 Case Definitions

For the next study, a new solid wall geometry (fig. 2, bottom) which gives a decelerating flow over the ramp with an extensive separation zone was created. From the same figure, a straightforward comparison with the CFDval2004 hump shape can be made. The solid wall of the new hump was generated using standard Bezier-Bernstein polynomials with 10 control points, as follows: (0.0,0.0), (0.1,0.0), (0.2,0.15), (0.4,0.18), (0.6,0.15), (0.61,0.0), (0.65,0.37), (0.66,-0.03), (0.8,0.0), (1.0,0.0). The numerical study was carried out with unit hump chord and symmetry conditions over the domain upper boundary. The inlet isentropic Mach number is 0.30 and the chord-based Reynolds number 6.35×10^6.

Concerning the steady suction parametric study, four design variables along with their lower and upper bounds have been defined, namely:

- the non-dimensional slot chord-wise location $\left(\hat{x}_{slot} = x_{slot}/c\right)$, in [0.64 , 0.68],
- the jet inclination $\left(\theta_{jet}\right)$, measured with respect to the local normal to the wall, in [30^o , 70^o],
- the non-dimensional slot width $\left(\hat{b}_{slot} = b_{slot}/c\right)$, in [0.001323 , 0.002457] and
- the non-dimensional suction mass flow rate $\left(\hat{\dot{m}}_{jet} = \dot{m}_{jet}/\dot{m}_{main}\right)$, in $[-0.25 \cdot 10^{-3}$, $-0.15 \cdot 10^{-3}]$; note that $\dot{m}_{main}$ is the mass flow rate passing through the half span duct, i.e. up to the symmetry boundary, and the negative sign denotes suction.

3.2 The Grid Generation Process

Though the parametric study-optimization could be carried out with user interference, the set up of an automated grid generation process, capable of remeshing the flow domain if one or more geometric design variables vary, is of primary importance. By possessing such a grid generation tool, the use of any optimization method (gradient-based, evolutionary algorithm, etc) is straightforward. The meshing process, on a step-by-step basis, is briefly described below.

Firstly, an unstructured grid is generated by neglecting the existence of the control slot. To increase the near wall flow modeling accuracy, structured layers are generated and the remaining domain (enclosed by the ending grid line of these layers, the inlet and outlet boundary, as well as the top-most domain boundary where symmetry flow conditions were imposed) is then filled with triangles generated using the advancing front algorithm. The quadrilateral elements in the structured-like part of the grid are split into two triangular elements each. This first step is carried out just once and the resulting grid must be modified accordingly whenever a slot (thus, a cavity) is to be attached.

By defining the slot geometry (width and jet inclination) and its location over the curved ramp, the cavity contour is first created; then an unstructured grid within the cavity is generated and attached to the main grid. It is beyond the scope of this paper to discuss on the cavity shape, since this should not affect the obtained results. In order to mesh the cavity, the same procedure (structured layers along its curved sidewalls, followed by a fully unstructured mesh in the remaining part of the domain) is used. To merge the two separately generated meshes (for the main domain and cavity), part of the main mesh close to the slot is removed and remeshed, after first rearranging the nodes distribution over the solid wall to match the boundary nodes of the cavity mesh. This procedure is illustrated in fig. 4. A close-up view of the final mesh, at the slot area, is shown in fig.5. It is obvious that this phase must be repeated whenever the slot geometry changes.

The aforementioned grid generation is the only non-parallelized part of the analysis of a candidate configuration. Once the mesh has been generated, it is decomposed into as many non-overlapping subdomains as the number of the available processors. For the grid partitioning, an in-house grid partitioner based on evolutionary algorithms is used [11].

3.3 Parametric Study - Optimization

During the parametric study-optimization presented below, the impact of the active flow control on the flow separation is quantified by the length of the separation region which is approximated by the distance between the two wall points at which the friction coefficient changes sign.

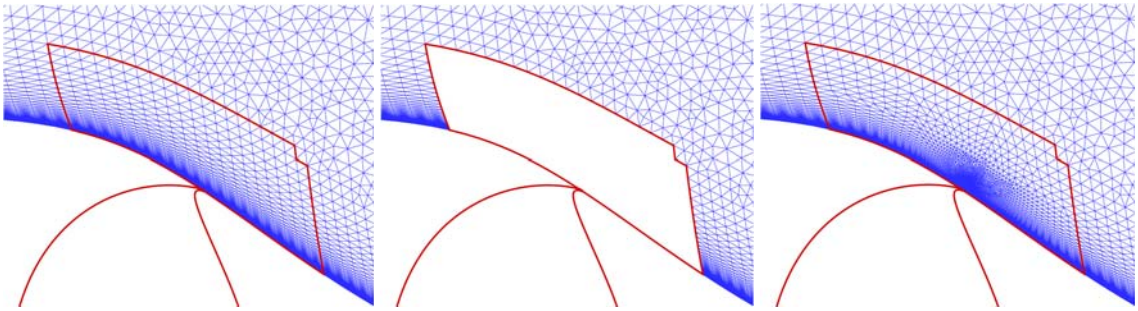

(a) (b) (c)

Figure 4: Grid adaptation over the slot region. The structured-like grid adjacent to the wall can be seen. In the sake of clarity, only the main flow domain is meshed.

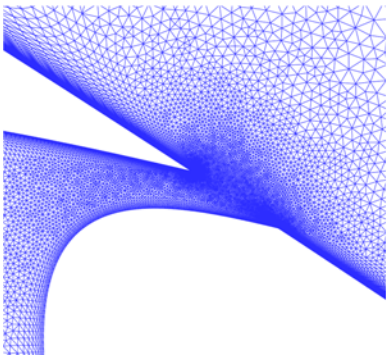

Figure 5: Close-up view of the final computational grid at the slot area. At the junction of the main and cavity meshes, the grid is fully unstructured.

The first study considers the effect of two parameters, namely the slot position and suction rate. The other two design variables were kept constant to $\theta_{jet} = 70^o$ and $\hat{b}_{slot} = 0.00189$. Five slot positions and five suction rates (forming an equidistant 2D grid, with 25 "experiments" in the R^2 design subspace) were tested and the best configuration among them $\left(\hat{x}_{slot} = 0.66,\ \hat{\dot{m}}_{jet} = -0.25 \cdot 10^{-3}\right)$ was selected. To better understand the flow control behaviour, fig.6, presents results from several runs, three of them with $\hat{\dot{m}}_{jet} = -0.25 \cdot 10^{-3}$ and varying $\hat{x}_{slot}$ values and three more with $\hat{x}_{slot} = 0.66$ and varying $\hat{\dot{m}}_{jet}$. With fixed slot position, any increase in the suction rate leads to reduction in the flow separation length. On the other hand, it is concluded that locating the slot over the ramp, just downstream of the separation onset, yields better performance.

For the "optimal" pair of values $\left(\hat{x}_{slot} = 0.66,\ \hat{\dot{m}}_{jet} = -0.25 \cdot 10^{-3}\right)$ and $\hat{b}_{slot} = 0.00189$, we then investigated the role of jet inclination. The search space [30^o , 70^o] for θ_{jet} was swept with an interval of 10^o and the smaller separation length was found for $\theta_{jet} = 50^o$. The variation in the separation length (normalized by the separation length of the uncontrolled case) around the "best" value $\theta_{jet} = 50^o$ is shown in fig. 7. The developed flow features in the vicinity of the suction slot for $\theta_{jet} = 30^o, 50^o$ *and* 70^o are shown in fig. 8.

At the final stage of this step-by-step optimization, the three previously investigated design variables were fixed at their "best" values $\left(\hat{x}_{slot} = 0.66,\ \hat{\dot{m}}_{jet} = -0.25 \cdot 10^{-3},\ \theta_{jet} = 50^o\right)$ and the slot width was allowed to vary between its lower and upper bound. A summary of this investigation is shown in fig. 9. Among the tested values, the slot width $\hat{b}_{slot} = 0.00189$ yields a considerable reduction (35%) in the separation length, compared to the uncontrolled case. No further interpolation was used to refine the so-called "optimal" set of design variables. In order to understand better the effect of active flow control, fig. 11 illustrates the friction coefficient distribution over the hump surface without and with control. The flow features of the uncontrolled and the "optimally" controlled case are shown in fig. 12.

In the present studies, the computational mesh (main mesh and cavity) for the controlled configurations had 85000 nodes/175000 triangles, on average. Working on 8 interconnected processors (XEON E5335 2quad core CPUs), the approximate CPU cost per analysis is 1h.

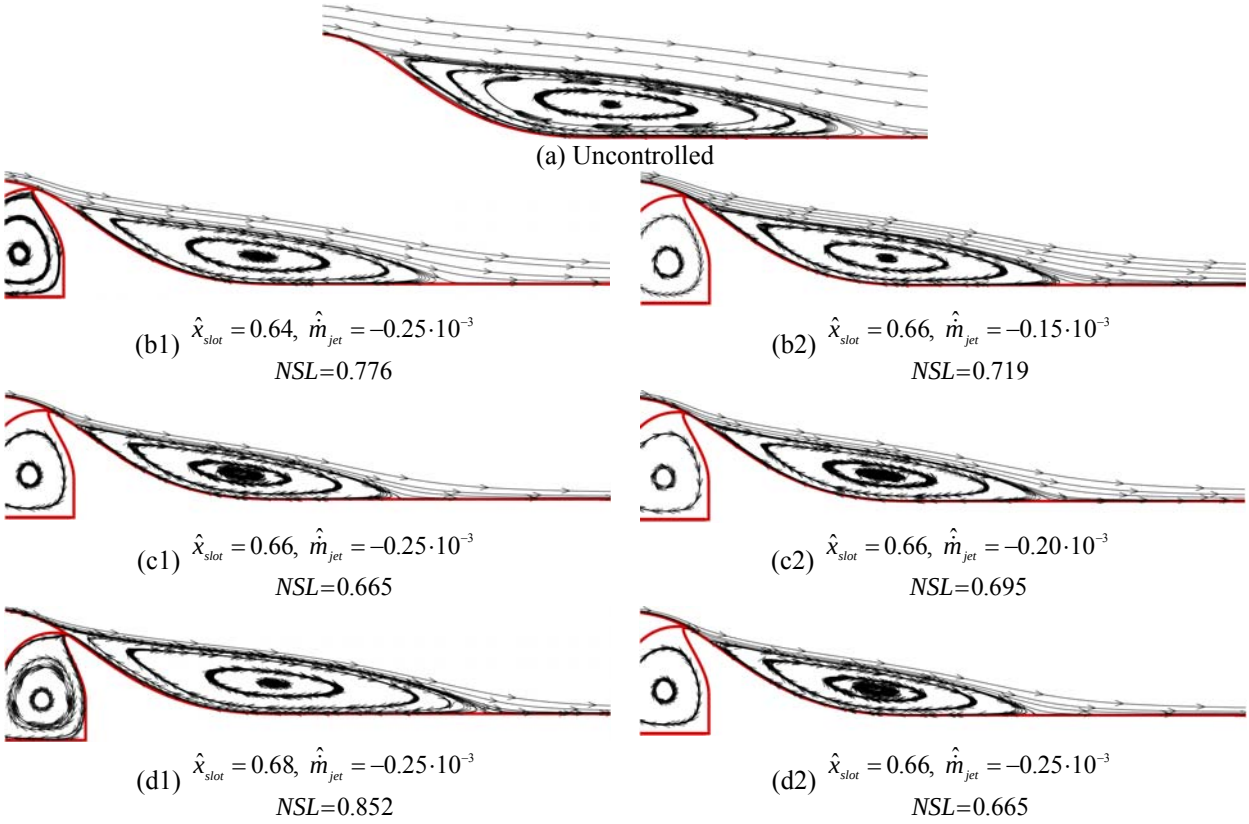

Figure 6: Steady Suction: Study of the impact of $\hat{x}_{slot}$ and $\hat{m}_{jet}$ on the separation length. With the two other design variables kept frozen ($\theta_{jet}=70^o$ and $\hat{b}_{slot}=0.00189$), the best performing configuration among the 5×5 tested ones is found; results for the "best" $\hat{m}_{jet}$ and varying $\hat{x}_{slot}$ (left column) and vice-versa (right column) are shown.

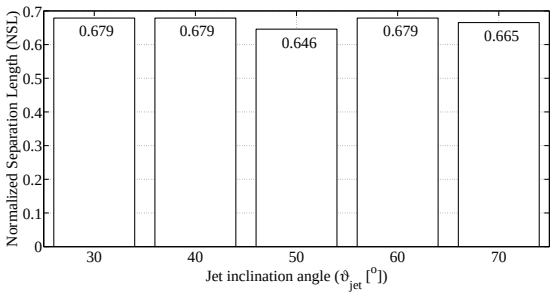

Figure 7: Steady Suction: Study of the impact of the jet inclination angle on the separation length, for $\hat{x}_{slot}=0.66,\ \hat{m}_{jet}=-0.25\cdot10^{-3},\ \hat{b}_{slot}=0.00189$.

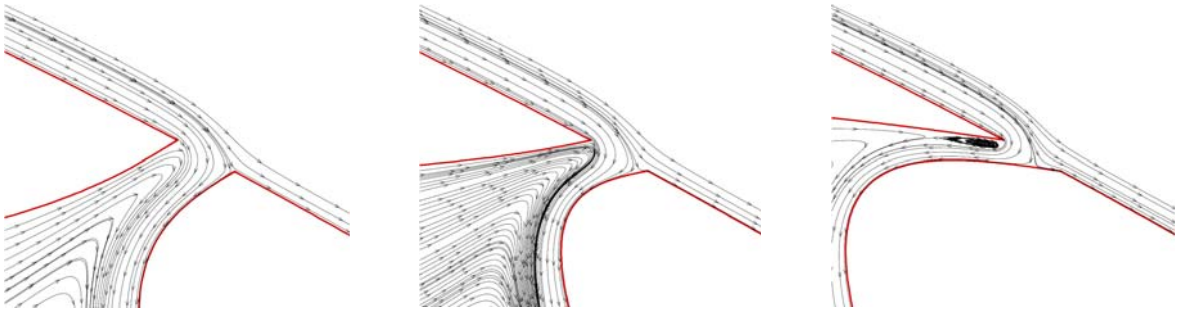

Figure 8: Steady Suction: Streamlines close to the suction slot is shown, for three different jet inclinations and $\hat{x}_{slot}=0.66,\ \hat{m}_{jet}=-0.25\cdot10^{-3},\ \hat{b}_{slot}=0.00189$

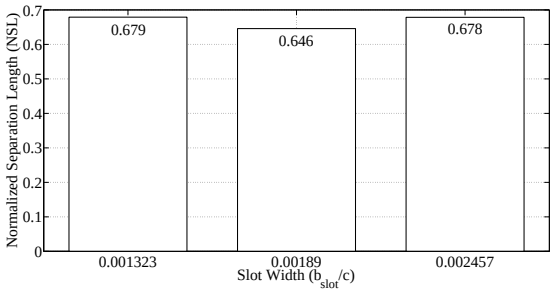

Figure 9: Steady Suction: Study of the impact of slot width on the separation length, for $\hat{x}_{slot} = 0.66,\ \hat{m}_{jet} = -0.25 \cdot 10^{-3},\ \theta_{jet} = 50^{o}$

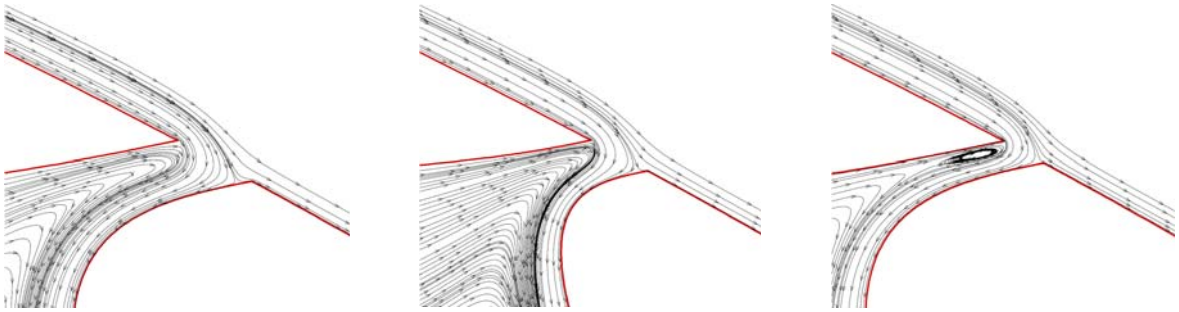

$\hat{b}_{slot} = 0.002457,\ NSL = 0.679$ $\hat{b}_{slot} = 0.00189,\ NSL = 0.646$ $\hat{b}_{slot} = 0.001323,\ NSL = 0.678$

Figure 10: Steady Suction: Streamlines close to the suction slot is shown, for three different slot widths and $\hat{x}_{slot} = 0.66,\ \hat{m}_{jet} = -0.25 \cdot 10^{-3},\ \theta_{jet} = 50^{o}$

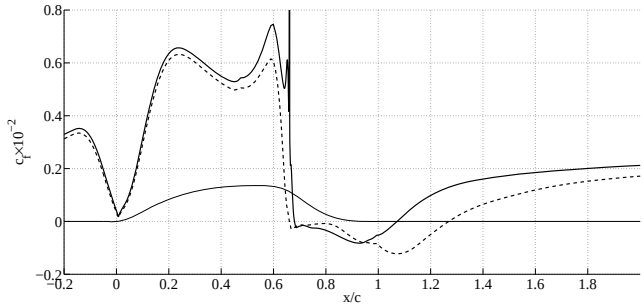

Figure 11: Distribution of friction coefficient for the "optimally" controlled configuration (continuous line) and the uncontrolled one (dashed line). The peak (negative) value of c_f at the separation zone was reduced by approximately 33%. The hump geometry is also shown.

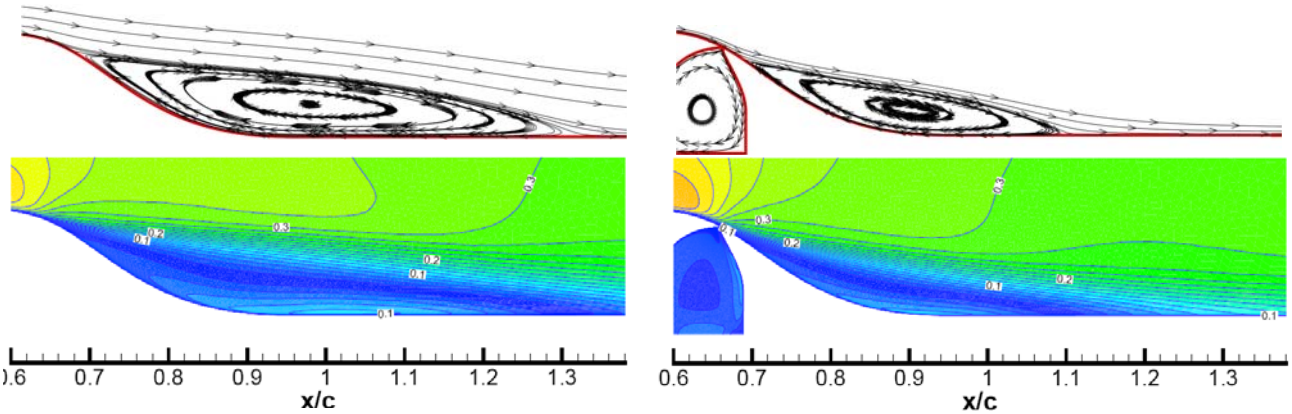

(a) Uncontrolled case.

(b) "Optimally" controlled case: $\left(\hat{x}_{slot} = 0.66,\ \hat{m}_{jet} = -0.25 \cdot 10^{-3},\ \theta_{jet} = 50^{o},\ \hat{b}_{slot} = 0.00189\right)$.

Figure 12: Uncontrolled case versus the "optimally" controlled one. The first row shows the streamlines at the separation region, while the second row illustrates the Mach number contour.

4 CONCLUSIONS

An active flow control optimization procedure based on the concept of ceteris paribus search, was presented. The adapted CFD software was validated on a well-known benchmark prior to the optimization. The step-by-step optimization entailed the development of an automated unstructured grid generator and the parametric study of a flow control configuration similar to the validation case, in which the slot location, suction rate, jet inclination and slot width were sequentially optimized to minimize the flow separation length. This step-by-step optimization led to approximately 35% decrease in the separation length. Though finding the global optimal solution cannot be guaranteed, this procedure was capable to locate a configuration with considerably low separation length, with low computational cost compared to that of e.g. an evolutionary algorithm. The latter may locate the global optimum within the design variables' bounds, at the expense of many calls to the evaluation software (grid generation tool and flow solver). Finally, it should be stated that the evaluation software is fully automated and, thus, ready for use along with an evolutionary algorithm or any other stochastic or gradient-based search method.

5 ACKNOWLEDGEMENTS

The third author was supported by a grant from the National Scholarship Foundation.

REFERENCES

[1] Buschmanna, M.H., Gad-El-Hak M. (2006), "Recent Developments in Scaling of Wall-bounded Flows", *Progress in Aerospace Sciences,* Vol. 42(5-6), pp. 419-467.
[2] Ekaterinaris, J. (2003), "Active Flow Control of Wing Separated Flow", *ASME FEDSM'03 Joint Fluids Engineering Conference,* Honolulu, Hawai, USA, 6–10 July 2003.
[3] Duvigneau, R., Visonneau, M. (2006), "Optimization of a Synthetic Jet Actuator for Aerodynamic Stall Control", *Computers & Fluids,* Vol. 35, pp. 624-638.
[4] Seifert, A., Darabi, A., Wygnanski, I. (1996), "Delay of Airfoil Stall by Periodic Excitation", *AIAA Journal,* Vol. 33(4), pp. 691-707.
[5] http://cfdval2004.larc.nasa.gov
[6] Lambropoulos, N.K., Koubogiannis, D.G., Giannakoglou, K.C. (2004), "Acceleration of a Navier-Stokes Equation Solver for Unstructured Grids Using Agglomeration Multigrid and Parallel Processing", *Comput. Methods Appl. Mech. Engng.,* Vol. 193, pp. 781-803.
[7] Roe, P.L. (1981), "Approximate Riemann Solvers, Parameter Vectors, and Difference Schemes", Journal of *Computational Physics,* Vol. 43, pp. 357-372.
[8] Venkatakrishnan, V. (1995), "Convergence to Steady State Solutions of the Euler Equations on Unstructured Grids with Limiters", *Journal of Computational Physics,* Vol. 118, pp. 120-130.
[9] Koubogiannis, D.G., Athanasiadis, A.N., Giannakoglou, K.C. (2003), "One- and Two-equation Turbulence Models for the Prediction of Complex Cascade Flows Using Unstructured Grids", *Computers & Fluid.,* Vol. 32, pp. 403-430.
[10] Rumsey, S.L., Gatski, T.B., Sellers, W.L, Vatsa, V.N., Viken, S.A. (2004), "Summary of the 2004 CFD Validation Workshop on Synthetic Jets and Turbulent Separation Control", *AIAA 2004-2217, 2nd AIAA Flow Control Conference,* June 28-July 1, Portland, OR.
[11] Giotis, A.P., Giannakoglou, K.C. (1998), "An Unstructured Grid Partitioning Method Based On Genetic Algorithms", *Advances in Engineering Software,* Vol. 29, pp. 129-138.